Fluxional Processes in Diamagnetic and Paramagnetic Allyl Dicarbonyl and 2-Methylallyl Dicarbonyl Molybdenum Histidinato Complexes as Revealed by Spectroscopic Data and Density Functional Calculations

Dave R. van Staveren,[b,c] Eckhard Bill,[b] Eberhard Bothe,[b] Michael Bühl,[c] Thomas Weyhermüller,[b] and Nils Metzler-Nolte*[a]

Abstract: This work describes a detailed study on the structure and dynamics of pseudooctahedral low-valent complexes of the type [Mo(His-N_ε-R)(η-2-R′-allyl)(CO)$_2$] (His = N_δ,N,O-L-histidinate; R = H, R′ = H (**1**); R = $C_2H_4CO_2Me$, R′ = H (**2**); R = H, R′ = Me (**3**); R = $C_2H_4CO_2Me$, R′ = Me (**4**)). These diamagnetic 18-electron complexes were comprehensively characterized spectroscopically and by X-ray crystallography. In the solid state, the (substituted) allyl ligand is in an *endo* position in all compounds, but it is *trans* to the His-N_δ atom in **1** and **2**, whereas it is *trans* to the carboxylate O atom for the 2-Me-allyl compounds **3** and **4**. In solution, both isomers are present in a solvent-dependent equilibrium. The third isomer (allyl *trans* to His-NH$_2$) is not spectroscopically observed in solution. This is in agreement with the results from density functional (DFT) computations (BPW 91 functional) for **1** and **3**, which predict a considerably higher energy (+ 6.3 and + 5.9 kJ mol^{-1}, respectively) for this isomer. A likely path for isomerization is calculated, which is consistent with the activation energy determined by variable temperature NMR measurements. At least for **3**, the preferred path involves several intermediates and a rotation of the 2-Me-allyl ligand. For the paramagnetic 17-electron congeners, DFT predicts the *exo* isomer of **3$^+$** with the 2-Me-allyl ligand *trans* to the carboxylate O atom to be by far the most stable isomer. For **1$^+$**, an *endo – exo* equilibrium between the isomers with the allyl ligand *trans* to the carboxylate O atom is suggested.

These suggestions are confirmed by EPR spectroscopy on the electrochemically generated species, which show signals for one- (**4**) and two- (**2**) metal-containing compounds. The appearance of the EPR spectra may be rationalized by inspection of the SOMOs from DFT calculations of the species in question. The notion of a metal-centered oxidation is also substantiated by IR spectroelectrochemistry and by UV/Vis spectra of the 17-electron complexes. Upon depleting the metal of electron density, the stretching vibrations of the carbonyl ligands shift more than 100 cm^{-1} to higher wavenumbers, and the carbonyl vibration of the metal-coordinated carboxylate shifts by about 50 cm^{-1}. A color change from yellow to green upon oxidation is observed visually and quantified by the appearance of a new band at 622 nm (**2$^+$**) and 546 nm (**4$^+$**), respectively.

[a] Prof. Dr. N. Metzler-Nolte
Pharmazeutisch-chemisches Institut
Universität Heidelberg
Im Neuenheimer Feld 364, 69120 Heidelberg (Germany)
Fax: (+49) 6221-54-64-41
E-mail: Nils.Metzler-Nolte@urz.uni-heidelberg.de

[b] Dr. D. R. van Staveren, Dr. E. Bill, Dr. E. Bothe, Dr. T. Weyhermüller
Max-Planck-Institut für Strahlenchemie
Stiftstrasse 34 – 36, 45470 Mülheim/Ruhr (Germany)

[c] Dr. D. R. van Staveren, Dr. M. Bühl
Max-Planck-Institut für Kohlenforschung
Kaiser-Wilhelm-Platz 1, 45470 Mülheim/Ruhr (Germany)

Introduction

The study of paramagnetic transition metal compounds is an active field in coordination chemistry and biological inorganic chemistry. Much of the interest in these compounds originates from the role of paramagnetic transition metal centers in metalloenzymes.[1, 2] A detailed understanding of transition metal trafficking and enzyme mechanism is often only possible through the in-depth study of the electronic state of the metal ions. In comparison to coordination complexes, the knowledge about paramagnetic *organometallic* compounds is limited. The high-spin state of manganocene derivatives is readily accessible and has been studied in detail.[3, 4] Maximum spin Cp (Cp = η-cyclopentadienyl) complexes of the 3d transition metals in general have been reviewed recently by Sitzmann.[5] The work on paramagnetic Cr compounds,

including some very interesting hydrides, has been pioneered by Theopold and Jolly.[6, 7] Some of these compounds are highly active olefin polymerization catalysts.[8] Electrochemically induced organometallic transformations were pioneered by Astruc,[9–11] and MoCp derivatives in particular have been recently studied.[12, 13] Most noteworthy, the work of Poli illustrates the rational design and synthesis of stable paramagnetic organometallic species.[14–16]

Many of those paramagnetic organometallic species are fairly sensitive. A 17-18-19-electron triad of stable isostructural organometallic FeCp complexes has been presented by Astruc and co-workers,[10] and Bennett et al. have reported a series of air-stable ruthenium alkene complexes with 17 and 18 electrons.[17] Although significant progress has been made recently, it is probably fair to say that tools for the comprehensive study of paramagnetic organometallic species are by far not as well established as for coordination compounds. This includes spectroscopic techniques in solution as well as computational work.[10, 18] Herein we present a comprehensive study on the molecular fluxionality, including mechanistic details, of organometallic Mo compounds in a diamagnetic 18-electron as well as a paramagnetic 17-electron state. Investigations on a related pair of compounds were reported by Poli and co-workers.[16, 19]

We have become interested in the properties of paramagnetic 17-electron species, which we hoped to generate from $[Mo(His)(allyl)(CO)_2]$ (allyl $= \eta\text{-}C_3H_5$) and derivatives, an interesting class of compounds that we have recently investigated.[20] The parent compound $[Mo(His)(allyl)(CO)_2]$ (**1**) was synthesized and partly characterized 20 years ago by Beck and co-workers in their effort to coordinate organometallic fragments (here $[Mo(allyl)(CO)_2]$) to amino acids (in this case three donor atoms from the amino acid histidine).[21, 22] We were intrigued by the exceptional properties of this compound. Seen as a pseudooctahedral complex, the compound combines a Werner-type half (N and O ligands) with an organometallic half (allyl and CO ligands). Second, the chirality of the metal can readily be reversed by the use of enantiomerically pure L- or D-His, which makes it an interesting candidate for the interaction with chiral biological ligands like peptides and DNA. In addition, this compound can be studied by a variety of spectroscopic techniques including IR spectroscopy of the carbonyl ligands and electrochemistry. Our group has pursued the synthesis of biomolecules like peptides and DNA analogues with covalently attached transition metal complexes.[20, 23–29] To this end, a suitable handle for binding the transition metal fragment to the biomolecules must be available. Reaction of an activated acid derivative with the N-terminus of a synthetic peptide is the most popular method, especially for solid-phase peptide synthesis, although a Pd-catalyzed Sonogashira coupling proved to be a versatile and flexible synthetic alternative in our hands.[25, 26] To produce a suitable acid derivative, we found that complex **1** may readily be substituted with a propionic acid side chain at the His-N_ε nitrogen atom.[20] This propionic acid methyl ester derivative was much more soluble in organic solvents than the parent compound **1**. Good solubility, together with the excellent stability of this air-

and water-stable organometallic compound and its favorable spectroscopic properties made it an ideal object for a detailed spectroscopic study. As expected, **1** and its derivatives readily undergo one-electron oxidation affording the corresponding paramagnetic 17-electron species.

During our studies of both the diamagnetic precursors and the oxidized paramagnetic complexes it became apparent that fluxionality of these species is a key issue. It is long known that the complex $[MoCp(\eta\text{-}allyl)(CO)_2]$ (**6**) exists in solution as a mixture of two isomers differing in the orientation of the allyl ligand (*exo* and *endo*, see Scheme 1).[30, 31] Since that time, fluxionality in diamagnetic complexes of the general formula
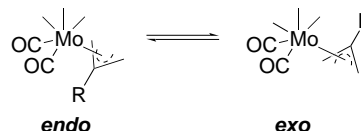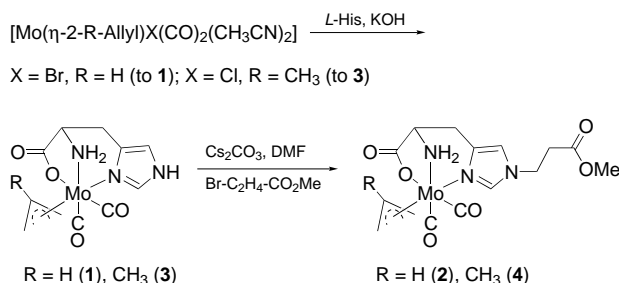

Scheme 1.

$[M(\eta\text{-}allyl)(CO)_2L_2X]$ (M $=$ Cr, Mo, W, see reference [32] for MLX nomenclature), of which compound **6** is just a very special case, has been studied in some detail by NMR spectroscopy in solution.[33–35] In the general case of $L_2X \neq$ Cp, a second fluxional process may come into play, namely a trigonal twist of the L_2X ligand plane with respect to the $(\eta\text{-}allyl)(CO)_2$ plane. The stereochemical implications of fluxional processes in $[M(\eta\text{-}allyl)(CO)_2L_2X]$ have been discussed, but all complexes investigated so far were either achiral or racemic mixtures.[35] In the chiral complex **1**, which is easily obtained enantiomerically pure, three different orientations of the His ligand with respect to the $(allyl)(CO)_2$ plane are possible. Furthermore, very little is known about the presence of rotational isomers (either allyl rotation or trigonal twist) in related one-electron-oxidized species,[36, 37] let alone about the parameters that might cause such fluxionality in paramagnetic compounds $[Mo\text{-}(\eta\text{-}allyl)(CO)_2L_2X]^+$. All of these issues are addressed in this work.

First, we present our findings on different fluxional processes in methyl propionate derivatives **2** and **4**, based on structures in the solid state and dynamic NMR spectroscopy in solution. These findings are augmented with a density functional (DFT) study of the potential energy surfaces of the parent species **1** and **3**. Second, we report on the characterization of the oxidized, paramagnetic 17-electron species **2⁺** and **4⁺**, calling special attention to fluxional behavior in solution, as revealed by detailed variable-temperature spectroelectrochemical studies. Further insight into the electronic situation of the paramagnetic 17-electron species is obtained from EPR spectroscopy at low temperature and from DFT calculations. The combined experimental and theoretical evidence strongly supports the occurrence of *different* fluxional processes in all species studied, and suggests that the population of the various isomers differs substantially between the 17-electron radicals and their 18-electron precursors.

Results and Discussion

Syntheses: The synthesis of complexes **1–4** is shown in Scheme 2. The reaction of [Mo(allyl)(Br)(CO)$_2$(MeCN)$_2$] with equimolar amounts of L-histidine and KOH in a MeOH/H$_2$O mixture at room temperature yields **1** in excellent yield. This method is more convenient than the previously reported route,[21] which consists of reacting

[Mo(η-2-R-Allyl)X(CO)$_2$(CH$_3$CN)$_2$] $\xrightarrow{\text{L-His, KOH}}$

X = Br, R = H (to **1**); X = Cl, R = CH$_3$ (to **3**)

Scheme 2. Synthesis of **1–4**.

K[Mo(His)(CO)$_3$] with allyl bromide, because this tris-carbonyl compound is highly sensitive towards dioxygen. The yield and purity of **1** synthesized and isolated by the new route were higher than with that previously reported. By reacting **1** at 80 °C for 2 h with 3-bromomethyl propionate in DMF in the presence of Cs$_2$CO$_3$, compound **2** is obtained in good yield after purification by preparative HPLC.[20]

Complex **3** is obtained in good yield by reacting [Mo(2-Me-allyl)(Cl)(CO)$_2$(MeCN)$_2$] with stoichiometric amounts of L-histidine and CsOH · H$_2$O in EtOH (Scheme 2). In contrast to the synthesis of **1**, EtOH was used in this case rather than MeOH because **3** is much more soluble in MeOH than **1** and does not precipitate from that solvent. Similar to the synthesis of **2**, complex **4** was obtained by reacting **3** with 3-bromomethyl propionate in DMF in the presence of Cs$_2$CO$_3$ for 2 h at 80 °C, followed by purification by preparative HPLC.

Solid-state structures: Single crystals suitable for X-ray structure determination were obtained for all compounds. We have recently published the X-ray crystal structure of **2** · 2MeOH.[20] ORTEP representations of **1** · MeOH, **3**, and **4** are depicted in Figures 1, 2, and 3, respectively. Selected geometric information is summarized in Table 1. As far as possible, a similar labeling scheme was employed for all molecules to facilitate the discussion. The unit cell of **3** contains two crystallographically inequivalent molecules, which display only slightly different bond lengths and angles. Because all corresponding bond lengths and angles of these two molecules are equal within experimental error, only the data for one of the molecules are presented in Table 1 and discussed here. For hydrogen-bonding interactions (vide infra), both molecules will be treated and atoms belonging to the second molecule will be denoted with a prime.

The coordination sphere around the Mo atoms in **1**, **3**, and **4** consists of identical donor atoms, namely two carbonyl ligands, three carbon atoms from an allyl (**1**) or 2-Me-allyl (**3** and **4**) ligand and the carboxylato oxygen atom, amine nitrogen atom, and nitrogen atom N$_\delta$ of either a histidine (**1**
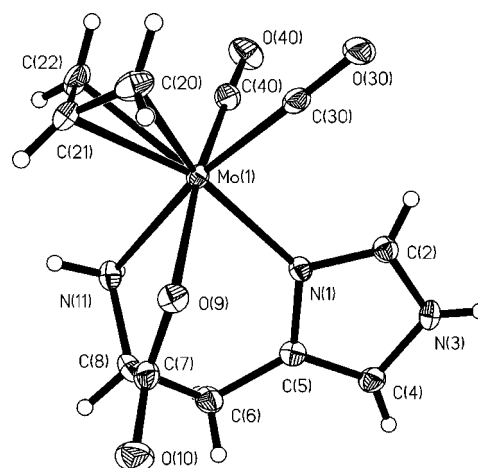
Figure 1. Structure of **1** · MeOH (ORTEP plot; thermal ellipsoids at 50 % probability level). The disordered MeOH molecule has been omitted for clarity.
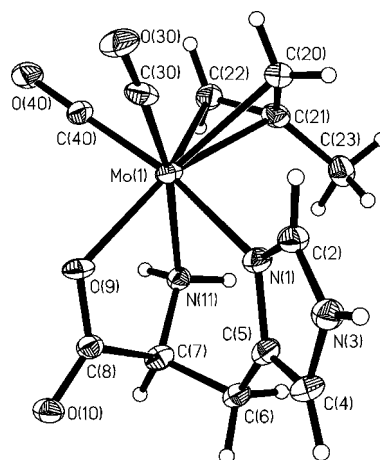
Figure 2. Structure of one of the independent molecules of **3** (ORTEP plot; thermal ellipsoids at 50 % probability level). The second crystallographically inequivalent molecule displays the same bond lengths and angles within 3σ.
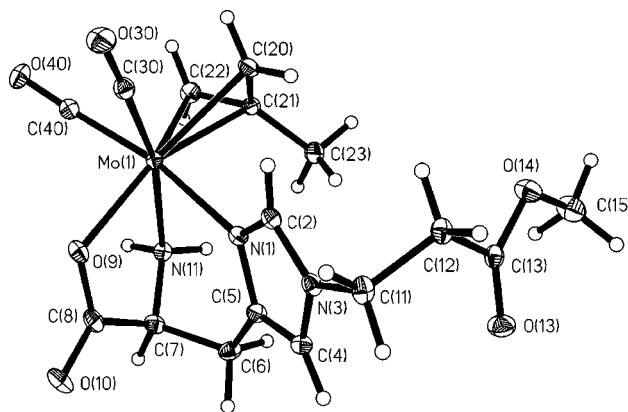
Figure 3. Structure of **4** (ORTEP plot; thermal ellipsoids at 50 % probability level).

and **3**) or N$_\varepsilon$-substituted histidine (**4**). The Mo(allyl)(CO)$_2$ (**1**) and Mo(2-Me-allyl)(CO)$_2$ (**3** and **4**) moieties are in a facial arrangement with the terminal CH$_2$ carbon atoms of the allyl or 2-Me-allyl ligand oriented towards the carbonyl ligands. Such a conformation has been shown to be energetically

Table 1. Selected bond lengths [Å] for **1** · MeOH, **2**, **3** (only one molecule, see text), **4**, and **5** · H$_2$O.

	1 · MeOH	**2**[a]	**3**	**4**	**5** · H$_2$O
Mo(1)−N(1)	2.217(2)	2.216(2)	2.254(5)	2.2699(11)	2.286(4)
Mo(1)−O(9)	2.222(2)	2.214(2)	2.150(5)	2.1517(11)	2.240(3)
Mo(1)−N(11)	2.272(2)	2.256(2)	2.276(5)	2.2711(12)	2.290(4)
Mo(1)−C(30)	1.945(2)	1.944(3)	1.955(7)	1.969(2)	1.916(4)
Mo(1)−C(40)	1.948(2)	1.945(3)	1.936(6)	1.951(2)	1.917(5)
Mo(1)−C(50)					1.946(5)
Mo(1)−C(20)	2.326(2)	2.328(3)	2.336(7)	2.337(2)	
Mo(1)−C(21)	2.212(3)	2.209(2)	2.216(7)	2.225(2)	
Mo(1)−C(22)	2.320(2)	2.328(3)	2.319(7)	2.304(2)	

[a] Data taken from reference [20], numbering scheme adjusted.

favored by EHMO (extended Hückel molecular orbital) calculations[38] and is observed in all solid-state structures of this type reported thus far (representative examples for allyl compounds[35, 38–42] and Me-allyl compounds[43–47]).

All of the Mo donor atom bond lengths in **1** · MeOH are equal within 3σ to those in the reported X-ray crystal structure of **2** · 2MeOH, despite short O · · · O contacts of the two MeOH molecules with the carboxylate group of the N$_\varepsilon$-substituted histidine in the latter structure. Therefore, bond lengths of **2** will not be discussed in relation to the structures presented in this study. Likewise, the Mo donor atom bond lengths of **3** and **4** are also equal within experimental error and therefore will not be discussed separately.

Apart from hydrogen bonds to MeOH molecules in **2**, there are no additional intermolecular contacts. For **1**, the molecules are arranged in a three-dimensional network with hydrogen-bond interactions between N(3) and O(9) (N · · · O contact 2.785 Å). The hydrogen-bonding pattern of **3** is more complicated. The carboxylate group of each crystallographically independent molecule is involved in one short and one longer hydrogen bond. The longer hydrogen bonds are between symmetry-related molecules, whereas short hydrogen bonds form between crystallographically independent molecules. Strong hydrogen bonds exist between N(3) and O(9) (N · · · O contact 2.813 Å and between N(3)′ and O(10)′ ((N · · · O contact 2.811 Å). Weaker hydrogen bonds are present between O(10) and N(11)′ ((N · · · O contact 3.167 Å and between O(10)′ and N(11) (N · · · O contact 2.913 Å).

Even at first glance, an interesting conformational difference between the allyl and the 2-Me-allyl ligand structures is evident. While the allyl ligand occupies a position *trans* to the N$_\delta$ nitrogen atom of the (substituted) histidine, the 2-Me-allyl ligand is located *trans* to the carboxylate oxygen atom of the amino acid. The electronic properties of the allyl ligand are changed by introduction of a methyl group on its central carbon atom, apparently resulting in a pronounced conformational change in the solid state. We believe that this is an electronic effect and not caused by crystal packing because it occurs in both groups of compounds with and without substituents on the His ligand, which have different space groups and crystal packing. Conformational differences of this kind were not observed in allyl/Me-allyl structures so far, for instance with bipyridyl[48] or phenanthroline ligands.[45] Indeed, they may only be observable at all in a completely unsymmetrical environment such as in **1**–**4**.

The different conformation of the allyl complexes in comparison to the 2-Me-allyl complexes is also reflected in some of the bond lengths. As shown in Figures 1–3, the primary amino group in these three structures is always *trans* to a carbonyl ligand. Therefore, unsurprisingly, the Mo(1)−N(11) bond lengths of **1**, **3**, and **4** are very similar. The situation is completely different with the Mo(1)−O(9) and the Mo(1)−N(1) distances. Whereas these are 2.222(2) and 2.217(2) Å, respectively, in **1**, the Mo(1)−O(9) bond lengths are shorter by around 0.07 Å in **3** and **4**. Likewise, the Mo(1)−N(1) distances are significantly longer in **3** (2.254(5) Å) and **4** (2.2699(11) Å). These variations can be rationalized on the basis of the *trans* influence of the allyl ligands.

To identify the structural influence of allyl ligands unambiguously, we determined the crystal structure of the compound [Mo(His)(CO)$_3$]AsPh$_4$[21] **5**, which has only CO ligands coordinated to the Mo(His) core. This compound crystallizes as **5** · H$_2$O. The varying *trans* influence of the three different histidinate donor atoms on the Mo−CO distances is nicely illustrated in the solid-state structure of **5** · H$_2$O. An ORTEP representation of the anion of **5** is depicted in Figure 4, bond lengths and angles are included in Table 1. In the crystal lattice, compound **5** forms alternating layers of AsPh$_4^+$ ions and the anions · H$_2$O. The carboxylate group of **5** forms two hydrogen bonds to a neighboring amide group (N(3) · · · O(9) 2.805 Å) and a water molecule (O(10) · · · O(60) 2.751 Å). Furthermore, O(60) forms a weak hydrogen bond to one of the hydrogen atoms of a coordinated amide group (N · · · O contact 3.029 Å).
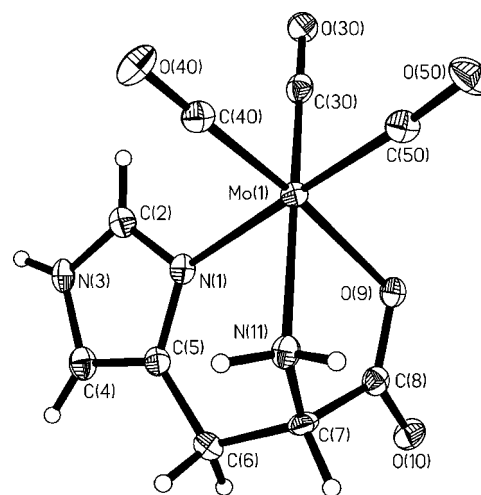

Figure 4. Structure of the anionic complex of **5** · H$_2$O (ORTEP plot; thermal ellipsoids at 50% probability level).

The Mo atom is coordinated in a distorted octahedral geometry by three carbonyl ligands and by the carboxylato oxygen atom, the N$_\delta$ nitrogen atom and the amino nitrogen atom of a tridentate histidine. The complex displays two shorter Mo−C(carbonyl) bond lengths at around 1.917(5) Å (Mo(1)−C(30) and Mo(1)−C(40)) and a slightly longer one (Mo(1)−C(50) 1.946(5) Å).[49] The carbonyl ligand with the longer Mo−C(carbonyl) distance Mo(1)−C(50) is *trans* to the

histidine N_δ nitrogen atom. This bond length elongation is likely due to the stronger π-acceptor ability of the imidazole compared to the amino and carboxylato group. All bond lengths between the Mo atom and the three histidine donor atoms are slightly longer in **5** than in **1**, **3**, and **4**. This is probably due to the overall negative charge of the metal complex in **5**.

Structure and fluxionality in solution: All compounds crystallize uniformly and there is no sign of disorder in the solid-state structures discussed so far. However, the situation is more complex in solution. For **1** and **2**, two sets of signals are observed in the ^{1}H NMR and ^{13}C NMR spectra, which indicates the presence of two isomers in solution. The histidine C–H protons of the two isomers in particular show a large chemical shift difference. For one of the isomers, $\delta({}^1\text{H})$ and $\delta({}^{13}\text{C})$ of the imidazole hydrogen and carbon atoms are very close to the values of histidine in D_2O. Furthermore, the ratio between the two isomers shows a marked solvent dependence. In solvents that are known to coordinate very well, like DMSO and DMF, the ratio between both isomers is close to 1:1, whereas it is about 4:1 in MeOH. Displacement of the imidazole ligand by a solvent molecule might therefore be a possible cause for the appearance of two isomers. However, the Mo–N_δ distance in the solid-state structures of **1** and **2** is the *shortest* of all three Mo–histidine donor atom bonds. Furthermore, the imidazole ligand would be most readily displaced in **5** because of the negative charge and the longest Mo–N bond length. However, both the ^{13}C and ^{1}H NMR spectra of **5** in DMSO show only one set of signals. Therefore, reversible Mo–N_δ bond cleavage is unlikely to be the cause for the observation of two isomers in **1**–**4**.

Allyl rotation, as observed in the complex [CpMo(allyl)(CO)$_2$] and analogues,[29, 30, 33] has been suggested by Beck and Meder to be the rotary motion observed spectroscopically in **1**.[22] Also, this paper reports that NMR spectra of **3** show only one set of resonances. This allyl rotary motion was later questioned on the basis of EHMO calculations.[38] The compounds in this study are well suited to put the two differing suggestions to an experimental test. If allyl rotation causes the observation of two isomers, then the 2-Me-allyl compounds are expected to show a higher activation energy for this process, simply due to the higher mass of the Me-allyl ligand. As detailed above, Beck and Meder's report on the simple NMR spectra of **3**[22] is at odds with our experience and this point certainly merits clarification.

The ^{1}H and ^{13}C NMR spectra of **3** and **4** show broadened resonances at room temperature in CD$_3$OD, [D$_3$]MeCN, and [D$_6$]DMSO, which is a first indication for coalescence. When the samples in CD$_3$CN and CD$_3$OD were cooled down, the ^{1}H NMR spectra of **3** and **4** indeed showed two sets of signals, at very similar chemical shifts to those of **1** and **2** at room temperature, which contain an unsubstituted allyl ligand. However, the ratio of the two isomers differs (Table 2). Variable-temperature NMR measurements were performed to determine the activation energy for the interconversion of the two isomers of **1**–**4**. The choice of solvents was limited by the low solubility of **1** and **3**, but **2** and **4** could be measured in different solvents to eliminate solvent effects (Table 2). In

Table 2. Isomer ratio and $\Delta G^{\pm}$ for their interconversion for **1**–**4** from variable-temperature ^{1}H NMR measurements.

Compound	Solvent	isomer ratio	$\Delta G^{\pm}$ [kJ mol^{-1}]
1	[D$_6$]DMSO	57/43[a]	66.7 ± 0.5
2	[D$_6$]DMSO	53/47[a]	66.9 ± 0.5
2	[D$_3$]MeCN	53/47[a]	66.7 ± 0.5
3	[D$_4$]MeOH	55/45[b]	58.6 ± 1.0
4	[D$_4$]MeOH	55/45[b]	58.5 ± 1.0
4	[D$_3$]MeCN	29/71[b]	60.4 ± 2.0

[a] At 300 K. [b] At 243 K

hindsight, the results in Table 2 also show that there is almost no solvent influence on $\Delta G^{\pm}$. Most important, the activation energy for interconversion in [D$_3$]MeCN is significantly *less* for the Me-allyl derivative **4** (60.4 ± 2.0 kJ mol^{-1}) than for the allyl compound **2** (66.7 ± 0.5 kJ mol^{-1}).[20] This result clearly argues against allyl rotation as the cause for isomerization.

In the solid-state structures, the Me-allyl and allyl ligands occupy the positions *trans* relative to the carboxylate group and to the N_δ atom, respectively. However, the NMR spectra of the allyl compounds **1** and **2** at ambient temperature are very similar to the NMR spectra of the 2-Me-allyl complexes **3** and **4** at lower temperature. It is therefore likely that the two observed isomers in solution have the conformations shown in the solid-state structures, namely the allyl or Me-allyl ligand *trans* to the carboxylate and *trans* to the N_δ atom. The large chemical shift differences of the imidazole hydrogen atom signals for the two isomers can be explained by the *trans* influence of the (substituted) allyl ligand. When the allyl or Me-allyl ligand is *trans* to the N_δ atom, the Mo–N_δ bond is shorter and stronger and, consequently, the imidazole hydrogen atom resonances are shifted downfield compared to those of the isomer in which a carbonyl group is *trans* to the N_δ atom. We conclude that a restricted trigonal twist (through pseudo-trigonal-prismatic transition structures) is the most probable rotary motion to interconvert these species in solution. This has been observed previously for related pseudooctahedral compounds with the Mo(allyl)(CO)$_2$ moiety.[34, 35, 39, 40] Also, the activation barriers of interconversion are in the range reported for trigonal twists of other pseudooctahedral Mo(allyl)(CO)$_2$ compounds.[39, 40] Unlike all previous examples with a higher symmetry, three different positions of the allyl ligand with respect to the Mo(His) plane are possible in **1**–**4**. Even in very clean ^{1}H NMR spectra we could not detect signals of a third isomer in solution. This suggests that the third isomer is considerably higher in energy than the other two. This suggestion is verified by theoretical calculations (vide infra).

In the case of [CpMo(allyl)(CO)$_2$], the different isomers stemming from allyl ligand rotation gave rise to two ^{95}Mo NMR signals.[33] Unfortunately, no ^{95}Mo NMR spectra could be recorded for compounds **1**–**4**; the asymmetry of the ligands probably causes rapid quadrupolar relaxation, leading to signals too broad to detect. In the following, we present theoretical results from DFT calculations that support and rationalize the spectroscopic findings described above.

DFT calculations on 1–4: To ensure that the chosen theoretical methods are capable of correctly describing the

energetics of molybdenum allyl complexes, the *endo* and *exo* isomers of [MoCp(allyl)(CO)$_2$] (**6**) have been studied. It is known from NMR studies that both exist as an equilibrium mixture at room temperature (*endo:exo* ratio 1:4, Scheme 1).[30, 33] At the BPW 91/II''//BP 86/SDD level of theory, the *endo* form is computed to be 1.6 kJ mol^{-1} less stable than the *exo* isomer. According to a Boltzmann distribution at room temperature, this corresponds to a 1:2 ratio, in excellent qualitative agreement with experiment.[50]

Subsequently, the energies of all six regioisomers **a–f** of [Mo(His)(allyl)(CO)$_2$] (**1**) and [Mo(His)(2-Me-allyl)(CO)$_2$] (**3**) were computed. These regioisomers differ in the relative orientation of the histidinate and (allyl)(CO)$_2$ moieties in the pseudooctahedral arrangement around Mo, as well as in the orientation of the allyl or Me-allyl ligand (*endo* or *exo*). The resulting structures are depicted schematically in Scheme 3. In addition, the energies of all species are summarized in Table 5 (see below).

The *endo* isomers **1d–f** are much higher in energy than the *exo* minima, of which two, **1a** and **1b**, are quite close in energy (within less than 1 kJ mol^{-1}), and the third, **1c**, is slightly less stable. These data support the identification of **1a** and **1b** as the two isomers that are observed in solution by NMR spectroscopy. Traces of **1c** might also be present, but most likely in amounts too small to be detected by NMR spectroscopy. This theoretical finding is in agreement with the NMR results described above.

Essentially the same results are obtained for the 2-Me-allyl derivative, [Mo(His)(2-Me-allyl)-(CO)$_2$] (**3**) (Scheme 3). Isomers **3a** and **3b** are computed to be most stable and are, thus, most likely the species found in solution. The energy difference is too small to determine the lowest energy conformer with certainty. As shown in Table 2 for the more soluble derivative **4**, the experimental situation is similar in that the ratio can be reversed by simply changing the solvent. It should be noted that although the differences in energy of **3a** and **3b** are rather small and the theoretical level chosen is certainly not sufficient to assess energy differences of a few tenths of a kJ mol^{-1}, it should nevertheless be adequate for the more qualitative purposes of this study.

According to dynamical NMR spectroscopy, the two isomers each observed for **1** and **3** interconvert on the experimental time scale in MeCN with barriers of 66.7 ± 0.5 and 58.6 ± 2.0 kJ mol^{-1}, respectively. In an attempt to rationalize the experimental find-
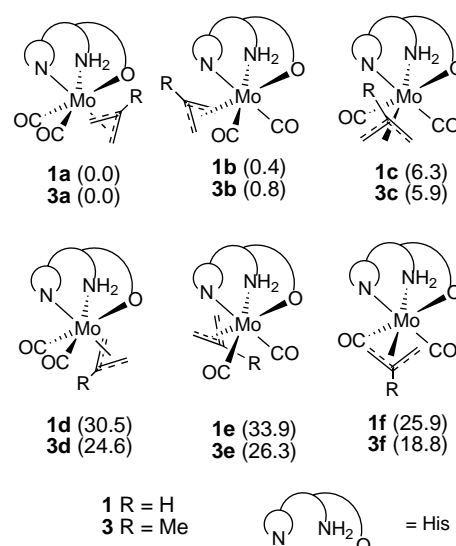
Scheme 3. The six regioisomers **a–f** of [Mo(His)(allyl)(CO)$_2$] (**1**) and [Mo(His)(2-Me-allyl)(CO)$_2$] (**3**). Energies are given in parentheses (see also Table 5).

ings and provide further support for the structural assignments, we computed a plausible path for this interconversion, namely the pseudorotation of the His and (allyl)(CO)$_2$ fragments through pseudo-trigonal prismatic transition states (path A, upper part of Scheme 4). For **1**, the computed barrier
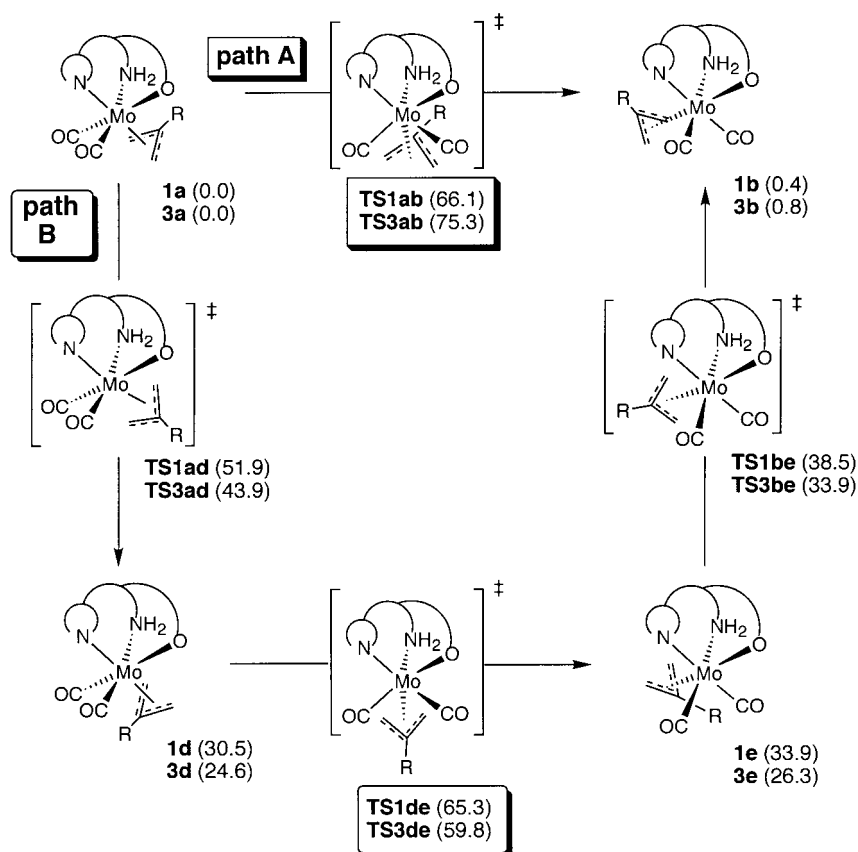
Scheme 4. Plausible paths for the interconversion of **1a** and **3a** into **1b** and **3b**: A) the pseudorotation of the His and (allyl)(CO)$_2$ fragments through pseudo-trigonal prismatic transition states; B) rotation of the coordinated allyl group to give the *endo* species **d**, followed by pseudorotation through a quasi-trigonal prismatic transition structure to give **e**, and finally rotation of the allyl moiety to yield the *exo* isomer **b**.

from this path, 66.1 kJ mol^{-1}, is virtually identical to the experimental number. A substantially higher value of 75.3 kJ mol^{-1} is obtained for the Me-allyl derivative **3**. The higher barrier for **3** versus **1** on path A is due to the increased steric bulk of the methyl group as it passes the histidine NH$_2$ moiety in **TS3ab** (closest NH$\cdots$HC contact 2.08 Å versus 2.22 Å in **TS1ab**). This result is in sharp contrast to that obtained by experiment, which displays a *lower* barrier for **3** than for **1**. Thus, a simple pseudorotation using path A cannot be reconciled with the experimental observations for **3**.[51]

Closer inspection of all isomers of **1** and **3** in Scheme 3 reveals that the *endo* isomers of the latter are generally lower in energy than those of the former. We assumed that the lower barrier for **3** might involve some of these *endo* isomers as intermediates of the interconversion. Indeed, a suitable reaction path was found computationally (path B, lower part in Scheme 4). This path consists of 1) rotation of the coordinated allyl group affording the *endo* species **d**, 2) pseudorotation through a quasi-trigonal prismatic transition structure affording **e**, and 3) rotation of the allyl moiety yielding the *exo* isomer **b**. In this sequence, the highest total activation energy is required for step 2). The corresponding barrier of 65.3 kJ mol^{-1} in the case of **1** is similar to, and even slightly lower, than that on path A. More importantly, the highest point on path B is 59.8 kJ mol^{-1} for **3**, which is approximately 6 kJ mol^{-1} lower than that for **1**. This finding is now fully consistent with the experimental data.

Path B thus represents a viable reaction sequence consistent with experimental data, substantiating the assignment of the two isomers of each **1** and **3**. The fluxional behavior of these isomers at higher temperatures is a complex process, involving possibly (for **3** most likely) at least two intermediates with *endo* orientation of the allyl group.

It should be noted that other pathways cannot fully be excluded, for instance those involving the remaining isomers **c** and **f**. It is unlikely, however, that the general conclusion regarding the highest barriers for **1** and **3** would be invalidated. On paths A and B, the allyl groups are always bonded in an η^3 fashion. Another possibility might involve η^1-bonded allyl intermediates. To test whether such η^1-bonded species could be competitive, a representative isomer (**1g**) has been optimized. The resulting structure is characterized by an $\alpha$-agostic Mo−H interaction[52] and is 130 kJ mol^{-1} higher in energy than **1a**. It is conceivable that strongly donating solvents might stabilize an η^1-form by coordination to the Mo center (at the empty site that is occupied by the α-agostic H atom in **1g**). Such a scenario, however, appears to be unlikely and therefore has not been further explored computationally.
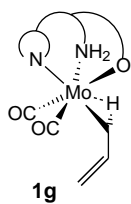
Our interest extends not only to the diamagnetic species **1**–**4**, but also to their paramagnetic one-electron-oxidized congeners. In the following, we describe the formation and spectroscopic investigations on **2**$^+$ and **4**$^+$. These studies are supplemented by a DFT treatment of **1**$^+$ and **3**$^+$.

Investigation of the paramagnetic 17-electron complexes: Variable-temperature electrochemistry: Because **2** and **4** are reasonably soluble in propionitrile even at low temperatures, all electrochemical investigations were carried out in that solvent. The cyclic voltammograms (CVs, 25°C, scan rate 200 mV s^{-1}) of both compounds exhibit a wave with reversible appearance at $E(1/2) = 86$ mV (**2**) and $E(1/2) = 25$ mV (**4**) versus ferrocene/ferrocenium (Fc/Fc$^+$). Controlled potential coulometry at 500 mV (**2**) and 600 mV (**4**) versus Fc/Fc$^+$, respectively, proves that this wave arises from a one-electron oxidation. In both cases, CVs before and after oxidation were identical, which demonstrates the reasonable stability of **2** and **4** in their reduced and oxidized forms. The current density function ($I_p/(SR)^{1/2}$; I_p = peak current density, SR = scan rate) of the cathodic and anodic peaks was found to be constant within 15% for a wide range of scan rates. This demonstrates that both compounds undergo unperturbed diffusive exchange with the electrode surface (2 mm glassy carbon and 0.05 mm Pt electrodes were used) and that adsorption phenomena are absent. Nevertheless, the oxidation of **2** and **4** does not proceed by an uncomplicated single reversible process.

For **2**, we have shown that two species must be present in the oxidized and reduced form, which are in rapid exchange on the electrochemical time scale.[20] At low temperatures, the exchange is slowed down and signals for both species can be detected. Upon warming the sample, a situation similar to coalescence in NMR spectroscopy is observed in the square wave voltammogram (SWV). Thermodynamic parameters including ΔG^0 (corresponding to equilibrium constants K) could be extracted from these measurements.[20] The underlying model assumes the presence of two isomers in *both* the oxidized and reduced forms of **2** (Scheme 5). A similar model can be applied to the Me-allyl derivative **4**.
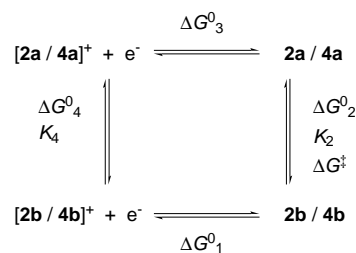
Scheme 5. The presence of two isomers in *both* the oxidized and reduced forms of **2** and **4** is assumed in the underlying model.

Unlike **2**, there was almost no evidence for two species of **4** even at −40°C (Figure 5). Only in SWVs at −55°C and higher scan rates the anodic scan exhibits a shoulder on the anodic side of the peak and at −75°C (the lowest temperature attainable) anodic and cathodic scans are quite symmetrical. This means that only at −75°C the equilibrium composition of the reduced form is maintained after oxidation at least for the time required for a cathodic scan. Already at −60°C, the isomer ratio was found to be constant for both scan directions over a wide range of scan rates for **2**. A related analysis for **4** reveals that the equilibrium isomer ratio is not perfectly "frozen" even at −75°C. The most favorable conditions for
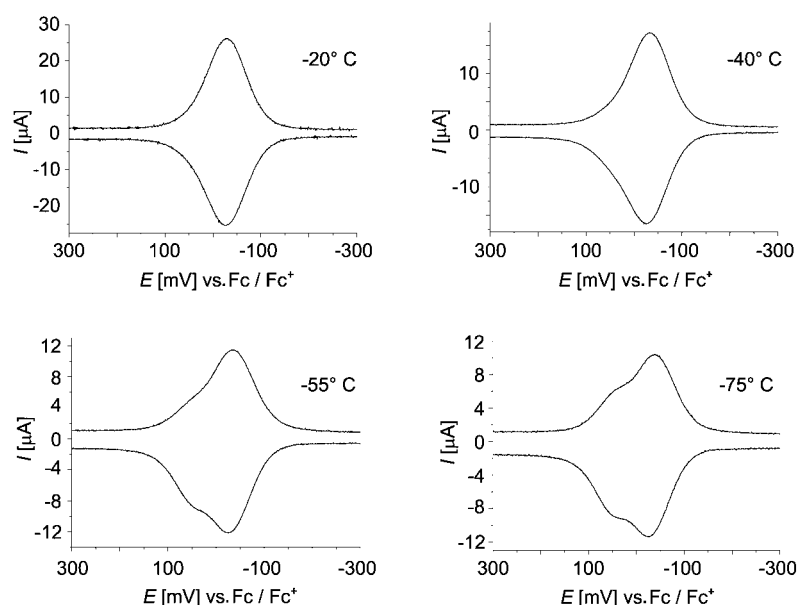
Figure 5. Square wave voltammograms of **4** at different temperatures.

IR spectroelectrochemistry: These investigations were performed on the methyl propionate-substituted compounds due to their better solubility in organic solvents. We stress again that **1** and **3** have very similar properties to **2** and **4**. Both **2** and **4** show a reversible one-electron oxidation at room temperature, although the situation is more complex at lower temperatures (vide supra). The CO vibrations of **2** and **4** were monitored during oxidation and subsequent re-reduction, performed at 0 °C using an OTTLE cell (Figure 6). In the neutral forms, **2** and **4** each show two carbonyl vibrations at 1933/1835 cm^{-1}

application of the "square scheme model" in Scheme 5 were anodic scans at high scan rates. Under these conditions, we find $\Delta G^0_2 = +0.57$ kJ mol^{-1} ($K_2 = 0.71$). From the curve-fitting procedure and a potential difference of 80 mV between the two species we then obtain $\Delta G^0_4 = -8.3$ kJ mol^{-1} ($K_4 = 150$). From the temperature dependence of the SWVs, further thermodynamic parameters ΔH and ΔS for **2** could be obtained. Unfortunately, ΔH and ΔS could not determined reliably for **4** because of the limited temperature range available. All parameters are summarized in Table 3.

Table 3. Summary of free reaction energy, enthalpy and entropy for both observable isomers of **2** and **4** in their reduced and oxidized forms from electrochemical data (see Scheme 5).

	2	**4**[a]
ΔG^0_1	-40.1 kJ mol^{-1}	n.d.
ΔG^0_2 (K)	-0.72 kJ mol^{-1} (1.5)	$+0.57$ kJ mol^{-1} (0.71)
ΔG^0_3	$+48.3$ kJ mol^{-1}	n.d.
ΔG^0_4 (K)	-7.5 kJ mol^{-1} (68)	-8.3 kJ mol^{-1} (150)
ΔH^0_2	-2.5 kJ mol^{-1}	n.d.
ΔH^0_4	-8.3 kJ mol^{-1}	n.d.
ΔS^0_2	-4.3 J K^{-1} mol^{-1}	n.d.
ΔS^0_4	-8.2 J K^{-1} mol^{-1}	n.d.

[a] n.d. = not determined.

The values in Table 3 indicate that for reduced **2**, the form with the *higher* redox potential is slightly favored in MeCN, whereas the oxidized form exhibits a pronounced preference for the species with the *lower* redox potential. In contrast, both the reduced and oxidized form of **4** prefer the species with the *lower* oxidation potential. In fact, a K_4 value of 150 means that there is basically only one species present of **4$^+$** in propionitrile solution. In a control experiment, we performed cathodic scans on a solution of **4$^+$**, obtained by bulk electrolysis at -10 °C. Indeed, only a single, narrow peak was observed at all temperatures, in agreement with the high value of K_4.
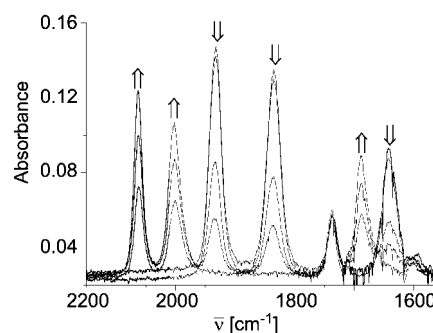

Figure 6. IR spectra (carbonyl stretching vibrations only) of **4** before and after oxidation and after re-reduction. Note the complete reversibility of the spectra after re-reduction (see text).

and 1932/1835 cm^{-1} in CH$_2$Cl$_2$, respectively. These are in the range reported for several other pseudooctahedral [Mo(allyl)(CO)$_2$] compounds.[35, 37, 40–42] Because two isomers exist in solution, four carbonyl vibrations were expected, but only two were observed. A plausible explanation is that apolar solvents, such as hexane or methylcyclopentane, are mandatory for obtaining small linewidths.[53] In CH$_2$Cl$_2$, all bands are significantly broadened, in this case leading to an overlap of signals from both isomers. Upon oxidation of **2** and **4**, the vibrations shift to 2065/2007 cm^{-1} and 2062/2002 cm^{-1}, respectively. Upon re-reduction, the original spectra are again observed (Figure 6).

Because there is only a marginal loss of intensity of the carbonyl and all other bands, we conclude that the oxidation of **2** and **4** is completely reversible at 0 °C for minutes. The frequency shift upon oxidation is of the same order of magnitude as observed previously for [Mo(allyl)(CO)$_2$L$_2$X] complexes (X = halogen, L$_2$ = didentate nitrogen-donor ligand).[37] A shift to higher wavenumbers upon oxidation is consistent with decreased $\pi - \pi^*$ backbonding as a consequence of decreased electron-availability at the metal.

Furthermore, the intensity of the vibrations of the oxidized forms is lower compared to that of the neutral forms. This is also consistent with the assumption of decreased backbonding as the intensity of carbonyl vibrations depends on the degree of "orbital following",[53-55] which is indeed decreased in a case where less metal-ligand backbonding occurs. Finally, the linewidths of the carbonyl vibrations of **2**+ and **4**+ are significantly smaller than in their reduced counterparts. This observation may be rationalized on the basis of the equilibrium constants of the neutral and oxidized forms (see Table 3). As calculated from temperature-dependent cyclic voltammetry experiments (vide supra), the equilibrium constant is 150 for **4**+, whereas it is 0.71 for **4**. Qualitatively, this means that in solution only one species is present for **4**+, whereas two isomers are present in a 60:40 ratio in the case of the neutral complex **4**. Since each of the isomers is expected to display slightly different carbonyl vibrations (as discussed above), the vibrations in the neutral form are probably broadened due to overlap of two vibrations from the two different isomers.

Upon oxidation, the $\nu_{C=O}$ vibration of the metal-coordinated carboxylate of **2** and **4** shifts from 1642 to 1689 cm^{-1}, whereas the ν_{CO} of the methyl ester is unaffected by the change in oxidation state. This behavior is quite expected and is the basis for our assignment of the bands.

UV/Vis spectroelectrochemistry: Compounds **1**–**4** are bright yellow compounds. Their color is due to an absorption maximum just below 400 nm that tails into the visible region of the spectrum. Upon electrochemical oxidation, solutions of **2** or **4** turn pale green. This change in color was quantified by UV/Vis spectroscopy during oxidation in a coulometry cuvet. Representative spectra of **2** and **2**+ are displayed in Figure 7 and the changes are marked by arrows. Upon oxidation, the

maximum at 375 nm is blue-shifted to 348 nm. However, a new absorption is observed at 622 nm with low intensity ($\varepsilon \approx$ 70 M^{-1}cm^{-1}). This new absorption is probably due to a forbidden transition with d–d character in the 17-electron species **2**+ and causes the pale green color. The plot in Figure 7 shows two isosbestic points at 383 nm and 456 nm. This means that two species (**2** to **2**+) interconvert directly without any intermediates. Similar spectral changes are observed upon one-electron oxidation of **4**. Two isosbestic points at 379 and 437 nm are observed, and a weak new band at 546 nm ($\varepsilon \approx$ 70 M^{-1}cm^{-1}) appears. UV/Vis data for **2**/**2**+ and **4**/**4**+ are summarized in Table 4.

These observations are not at odds with our previous

Table 4. Summary of UV/Vis data for **2** and **4** in their reduced and oxidized forms. Only the energy (λ_{max} in nm) and absorption coefficient (ε in M^{-1} cm^{-1}) for the lowest energy transition are given.

Complex	Solvent	λ_{max}	ε
2	MeOH	385	820
2	MeCN	375	840
2+	MeCN	622	70
4	MeOH	366	940
4	MeCN	353	1080
4+	MeCN	546	64

findings that at least two isomers for either species are present in solution. For one, the time scale of optical spectroscopy is much shorter than the rate constant for the rearrangement, which is observable in the slower electrochemistry. Therefore, the observed interconversion in the UV/Vis spectroelectrochemistry experiments is indeed directly from one species to another. Second, the UV/Vis spectra of the two isomers of **2** and **4** are presumably very similar and there is reasonable doubt that the two isomers were at all discernable by their optical spectra.

EPR spectroscopy: UV/Vis spectroscopic data suggest that the orbital situation for **2** and **4** is not identical, because the transitions with d–d character occur at markedly different wavelengths. EPR spectra of the oxidized species were recorded to gain further insight into the electronic properties of the oxidized species. A sample was prepared by controlled potential coulometry in MeCN at $-20\,^{\circ}$C, the solution transferred into an EPR tube under argon atmosphere and quickly frozen in liquid nitrogen. In view of the long time required for coulometry (10–15 min.) and subsequent rapid freezing it is likely that the oxidized compounds are observed in their equilibrium ratio at $-20\,^{\circ}$C. The X-band EPR resonances of **2**+ and **4**+ are not well separated. In addition, an isotropic signal at $g = 2.00-2.01$ was observed in ratios varying from preparation to preparation. Q-band EPR spectra are displayed in Figure 8 for **4**+ and in Figure 9 for **2**+ along with the simulations. The spectrum of **4** can be fitted with two components, an isotropic spectrum with a g value of around 2.007 and an axial spectrum with $g_\perp = 2.010$ and $g_\parallel = 2.005$. The two components were present in varying ratios in subsequent preparations (the isotropic:axial ratio is 8:92 in the spectrum shown in Figure 8) and saturation experiments
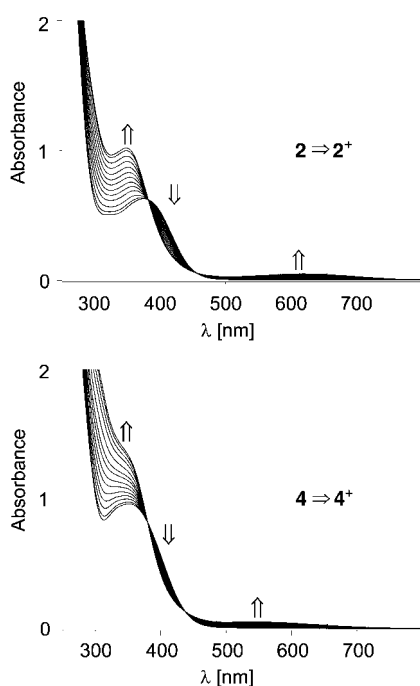

Figure 7. UV/Vis spectra of **2** and **4** during electrochemical oxidation.
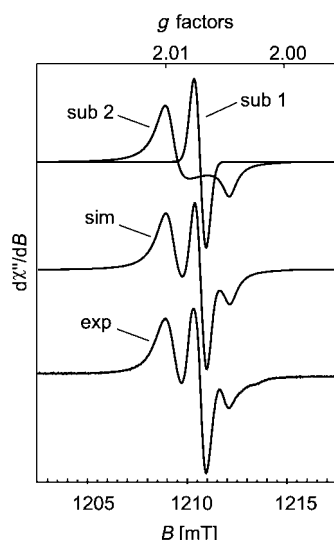
Figure 8. Q-band EPR spectrum of **4**⁺. Bottom: experimental spectrum, middle: simulated spectrum, top: subspectra. $T = 50$ K; power 9.62×10^{-3} mW; frequency 34.009702 GHz; modulation 0.51 mT.
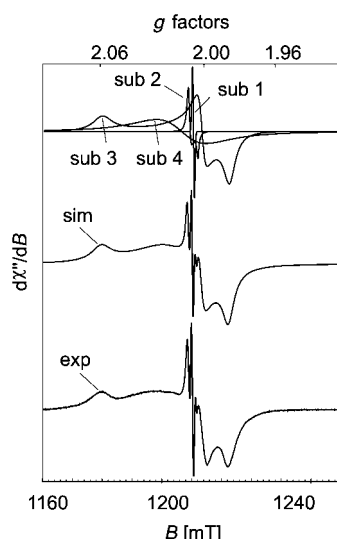

Figure 9. Q-band EPR spectrum of **2**⁺. Bottom: experimental spectrum, middle: simulated spectrum, top: subspectra. $T = 50$ K; power 9.62×10^{-3} mW; Modulation 0.82 mT.

underscored the point that the observed resonances do not belong to the same species.

The Q-band EPR spectrum of **2**⁺ (Figure 9) looks significantly more complicated and could only be fitted with four different subspectra. Interestingly, two components could be fitted with *g* values identical to **4**⁺. A third component with a rhombic spectrum was simulated ($g_x = 2.059$, $g_y = 2.003$, $g_z = 1.987$). The fourth subspectrum is a broad isotropic spectrum around $g = 2.014$ and a linewidth of 670 Gauss. This signal seems to originate from inhomogeneity, and because its *g* value is approximately the average of the three *g* values from the rhombic spectrum ($g_{av} = 2.016$), it is conceivable that both resonances originate from the same species. Under this assumption, the ratio between the signals is 0.1:0.8:99.1 (isotropic:axial:rhombic + broad).

Because of its appearance, a *g* value around 2.007 and its varying amount, it is likely that the isotropic signal originates from an organic decomposition product, possibly a free allyl or histidinyl radical. Compounds **2**⁺ and **4**⁺ are quite sensitive to dioxygen, and traces of dioxygen could not be excluded completely during sample preparation. Rhombic X-band EPR spectra were previously reported for electrochemically prepared [Mo(allyl)(CO)₂] complexes containing bipyridyl ligands.[36] Accordingly, the axial and rhombic spectra do likely originate from the oxidized metal complexes. Identical *g* values for the axial spectrum suggest similar species, but there is no obvious explanation for the spectral differences and the appearance of a rhombic signal for **2**⁺ at this stage. We have therefore performed DFT calculations on the radical cations **1**⁺–**4**⁺.

DFT calculations on the radical cations 1⁺–4⁺: To complement and rationalize the electrochemical and EPR findings pertinent to the redox behavior of the complexes in this study, all radical cations of isomers **1a**–**1f** have been studied computationally. Geometry optimizations were started from the structures of the respective neutral compounds. Upon oxidation, bonding between the Mo center and the histidine donor atoms is reinforced in all isomers, in particular to the carboxylic oxygen atom, which is computed to approach the metal by as much as 0.12 Å. In contrast, depleting the metal of electron density weakens backbonding to the π ligands, resulting in Mo—C distances elongated by approximately 0.02–0.09 Å. These findings are in qualitative agreement with results from IR spectroscopy, in particular the observed shift of the carbonyl bands and the coordinated His carboxylate group. The strong contact between the metal and the carboxylic oxygen apparently increases the *trans* influence of the latter over that of the imidazol nitrogen atom, rendering all isomers with the allyl ligand *trans* to O particularly favorable.

Interestingly, a completely different energetic sequence is obtained for the radical cations, as compared to the neutral precursors (Table 5). On going from **1** to **1**⁺, the *exo* isomers **a** and **b** switch their relative order of stability and **1b**⁺ is calculated to be the minimum structure for the radical cation. The energy difference of 5.5 kJ mol⁻¹ is in good agreement with the value obtained from variable-temperature electrochemistry on the methyl propionate derivative **2** (7.5 kJ mol⁻¹, vide supra). For **3**⁺, the energetic sequence differs from that of **1** in that the **e** isomer is calculated to be the most stable isomer. Isomers **b** and **e** both have the same geometry of the ligands around the Mo atom but differ in the orientation of the allyl ligand (*exo* or *endo*). Among the *endo* isomers, **1e** is substantially stabilized upon oxidation, to the extent that **1e**⁺

Table 5. Relative energies [kJ mol⁻¹] of neutral and cationic [Mo(His)-(CO)₂(η^3-C₃H₅)] complexes at the BPW 91/II//BP86/SDD+ZPE level.

Species/isomer	a	b	c	d	e	f
1	*0.0*	0.4	6.3	30.5	33.9	25.9
1⁺	5.5	*0.0*	15.3	13.8	3.2	25.3
3	*0.0*	0.8	5.9	24.6	26.3	18.8
3⁺	18.8	15.2	34.0	22.5	*0.0*	33.6

is only 3.2 kJ mol^{-1} above **1b**$^+$ (Table 5). Thus, the computations suggest that **1**$^+$ should exist as a mixture of two or three isomers at ambient temperature, and that the isomeric composition should be significantly different from that of **1** (assuming rapid equilibria between the low-energy isomers). For **3**$^+$, on the other hand, only one isomer will be observed experimentally.

The energy difference between **3e**$^+$ and **3a**$^+$ can be regarded as the actual difference that is determined from low temperature electrochemical experiments. It is quite conceivable that the 2-Me-allyl ligand of isomer **3b** undergoes a 180° rotation upon oxidation. In fact, DFT calculations on the activation barrier for interconversion between the neutral isomers **3a** and **3b** (vide supra) indicate the presence of *endo* intermediates during the interconversion process. It must be noted that the variable-temperature electrochemical investigations only permit to discriminate between different conformations of the allyl ligand (*trans* to the O atom or *trans* to N$_\delta$). A rotation of the allyl ligand (*exo* or *endo*) will not be observable by electrochemistry.

The results from DFT calculations provide an explanation for the observed EPR spectra of **2**$^+$ and **4**$^+$. The axial spectra of both compounds may arise from isomers **e**. **3e**$^+$ is by far the lowest energy isomer for **3**$^+$. For **1**$^+$, on the other hand, **1e**$^+$ is slightly higher in energy to **1b**$^+$. Hence, whereas only one isomer (**4e**$^+$) is present in a solution of **4**$^+$ and gives rise to an EPR signal, solutions of **2**$^+$ contain two species, namely **2e**$^+$ and **2b**$^+$. The main rhombic signal is then caused by **2b**$^+$, in accordance with DFT results that predicted it to be the major isomer for **2**$^+$.

An inspection of the SOMOs for **1e**$^+$, **3e**$^+$, and **3b**$^+$ provides a rationale for these observations (see Figure S1 in Supporting Information). *Both* carbonyl ligands are involved in backbonding in the SOMO of **3b**$^+$, and there is a weak interaction between the metal and the central carbon atom C(21) of the allyl ligand. The SOMOs of **1e**$^+$ and **3e**$^+$ are nearly identical with strong backbonding between the metal and *one* of the carbonyl ligands, together with contributions from the terminal carbon atoms C(20) and C(22) of the allyl moieties. Considering the similarity of the SOMOs of **1e**$^+$ and **3e**$^+$, the unpaired electron experiences an identical environment and very similar EPR spectra are anticipated. The SOMO for isomer **3b**$^+$ is notably different and a different EPR spectrum then comes as no surprise.

Conclusion

By combining the results from X-ray crystallography, spectroscopic, and low-temperature electrochemical investigations, as well as DFT calculations, we have been able to elucidate the structures and fluxional behavior of a number of Mo complexes of the type [Mo(His)(2-R-allyl)(CO)$_2$]. This is the first such detailed study including mechanistic details of the fluxional behavior of pseudooctahedral low-valent Mo complexes. It reveals remarkable differences in seemingly very similar organometallic compounds with R = H or CH$_3$. In their neutral forms, both compounds exist as an approximate 1:1 mixture of two isomers **a** and **b**, which have the allyl ligand in an *exo* position opposite to N$_\delta$ (**a**) or the carboxylate

O (**b**). The net process for interconversion of these isomers is a restricted trigonal twist. However, the exact mechanism of interconversion is more complicated and most probably different for **1** and **3**. For the former, direct rearrangement through a pseudo-trigonal-prismatic transition state is possible. For the latter, in contrast, a stepwise mechanism is indicated, involving *endo*-allyl isomers as intermediates along the reaction path. In the oxidized form, the *endo* isomer **e** (with the allyl group trans to the carboxylate O atom) is stabilized to the extent that it has by far the lowest energy of the Me-allyl species **3**$^+$. In the parent allyl derivative **1**$^+$, at least one isomer (**b**) is similar in energy and this fact is also reflected by more complicated EPR spectra. Previous work on [Mo(allyl)(CO)$_2$] complexes with additional bipyridyl and chelating phosphine ligands[35] shows that these compounds were fluxional in solution as shown by NMR spectroscopy, but only one isomer was observed in the oxidized form. In contrast, we were able to investigate the fluxionality, relative energies and the mechanisms of interconversion also of the paramagnetic 17-electron species in this study.

A comparison can be made to [Mo(Cp)(allyl)] compounds. The compound [Mo(Cp)(allyl)(CO)$_2$] (**6**), which is isolobal with [Mo(His)(allyl)(CO)$_2$], is one of the early examples of a fluxional organometallic compound. Fluxionality in **6** refers to allyl rotation (*exo* and *endo*) only. Very recently, Bitterwolf and co-workers demonstrated that the *exo* isomer is formed preferentially upon irradiation with $\lambda > 400$ nm at 90 K, whereas at 360 nm $< \lambda < 400$ nm, the *endo* isomer is enriched.[56] At even higher energies, photochemical loss of CO is observed. The behavior of [Mo(Cp)(η^3-allyl)(CO)$_2$] and [Mo(Cp)(η^1-allyl)(CO)$_3$] at cryogenic temperatures, as well as their interconversion, was studied in detail by Limberg and co-workers.[57] Poli et al. have studied equilibria between different isomers of [Mo(Cp)(allyl)(η^4-butadiene)].[16, 19] Again, allyl rotation is observed along with isomerization of the butadiene ligand (s-*cis* and s-*trans*). In their system, the allyl-*exo* conformation is favored for the 18-electron species, whereas the allyl-*endo* conformation is the most stable isomer for the 17-electron congener. Intermediates with η^1 coordination of the allyl ligand were considered unlikely on the basis of the measured activation energy for the rearrangement. Even under cryogenic conditions, no η^1 intermediate could be detected.[57] Our work demonstrates that substituents on the allyl ligand have a decisive influence on the energetic order of different isomers. Moreover, rotation about the Mo–Cp axis—which is the equivalent of a trigonal twist in **1** or **3**—is a low-energy process too rapid to be observed in Mo(Cp) compounds. Thus, although they are isolobal and superficially very similar, the [Mo(His)(allyl)] compounds in this study have very little in common with the [Mo(Cp)(allyl)] systems mentioned above as far as molecular structures and dynamics are concerned.

For applications in bioorganometallic chemistry, the compounds studied herein have attractive properties, namely very good stability even in aqueous, aerobic media and favorable spectroscopic properties. Furthermore, they can be readily substituted with suitable handles for conjugation to biomolecules like amino acids and peptides. Studies along these lines are in progress in our group and will be reported soon.

Experimental Section

General: All syntheses and manipulations were performed using standard Schlenck techniques under an atmosphere of argon. [Mo(allyl)(Br)(CO)$_2$-(MeCN)$_2$] and [Mo(2-Me-allyl)(Cl)(CO)$_2$(MeCN)$_2$] were prepared according to literature procedures.[58] All other chemicals were purchased from commercial suppliers and used as received, enantiomerically pure L-histidine was used throughout. Elemental analyses were carried out by H. Kolbe, Analytisches Laboratorium, Mülheim. IR spectra were recorded on a Perkin Elmer System 2000 instrument as KBr disks, additionally in CH$_2$Cl$_2$ solution where indicated. Wavenumbers are given in cm^{-1}. A Hewlett-Packard 8453 spectrometer was used for UV/Vis and spectroelectrochemistry. Mass spectra were recorded by the mass spectrometry service group, Mülheim, on a MAT 8200 (Finnigan GmbH, Bremen) instrument (EI, 70 eV) or on a MAT 95 (Finnigan GmbH, Bremen) instrument (ESI, CH$_3$OH solution, positive-ion detection mode). Only characteristic fragments are given with intensities (%) and possible composition in brackets. Cyclic voltammograms were obtained with a three-electrode cell and an EG&G Princeton Applied Research model 273 A potentiostat. An Ag/AgNO$_3$ (0.01 mol L^{-1} in AgNO$_3$) reference electrode, a glass carbon disk working electrode of 2 mm diameter and a Pt wire counter electrode was used. Standard square wave voltammograms (SWVs) were recorded with a step height of 1 mV, 25 mV pulse amplitude and 40 Hz frequency. CH$_2$Cl$_2$, MeCN or EtCN solutions (approximately 10^{-4} mol L^{-1}) contained 0.1 mol L^{-1} Bu$_4$NPF$_6$ as supporting electrolyte. Ferrocene was added in excess as an internal reference. Controlled potential coulometry measurements (for preparative purposes as well as for UV/Vis spectroelectrochemical studies) were performed with the same supporting electrolytes by employing the above mentioned potentiostat, using a Pt grid as working electrode, a Pt brush auxiliary electrode separated from the working electrode compartment by a vycor frit and an Ag/AgNO$_3$ (0.01M AgNO$_3$ in MeCN) reference electrode. Thin-layer IR spectroelectrochemical measurements were performed by using an OTTLE cell of 0.17 mm optical path-length consisting of a Pt grid working electrode, a glassy carbon counter-electrode and an Ag-wire as "quasi-reference electrode". Standard NMR spectra were recorded at 300 K on a Bruker ARX 250 (^{1}H at 250.13 MHz and ^{13}C{^{1}H}), DRX 400 (^{1}H at 400.13 MHz, ^{13}C{^{1}H} and 2D spectra) and DRX 500 (^{1}H at 500.13 MHz, ^{13}C{^{1}H}, ^{95}Mo, 2D). ^{1}H and ^{13}C{^{1}H} spectra were referenced to TMS, using the ^{13}C signals or the residual proton signals of the deuterated solvents as internal standards (CDCl$_3$ ≡ 7.24 (^{1}H) and 77.0 (^{13}C), DMSO ≡ 2.49 (^{1}H) and 39.5 (^{13}C)). Positive chemical shift values δ indicate a downfield shift from the standard, only the absolute values of coupling constants are given in Hz. All resonances were assigned by 2D NMR (H-H-COSY and ^{1}H-^{13}C-HMQC for ^{1}J and long-range couplings). Preparative high performance liquid chromatography (HPLC) purification was performed by using a Macherey & Nagel Nucleosil 7-C18 column (250 × 21 mm) using a MeOH/H$_2$O (1:1 v/v) mixture as the eluent.

Synthesis

1: A solution of L-histidine (1.73 g, 11.0 mmol) and KOH (0.62 g, 11.0 mmol) in H$_2$O (30 mL) was added to a solution of [Mo(allyl)(Br)-(CO)$_2$(MeCN)$_2$] (3.95 g, 11.0 mmol) in MeOH (35 mL). After the mixture had been stirred for 45 min, it was concentrated in vacuo to about 20 mL. The yellow precipitate was isolated by filtration, washed with H$_2$O (15 mL) and diethyl ether (15 mL) and dried in vacuo. Yield: 3.70 g (97%). X-ray quality crystals of **1**·MeOH were obtained by evaporation of a H$_2$O/MeOH (1/3 v/v) solution under a stream of argon. ^{1}H NMR (400.1 MHz, [D$_6$]DMSO): δ = 8.56/7.94 (s, 1H; N$_2$CH$_{His}$), 7.03/6.84 (s, 1H; CH$_{His}$), 4.71/3.93 (br, 1H; NH$_2$), 4.05/3.90 (br, 1H; NH$_2$), 3.50 (m, 1H; C$_\alpha$H), 2.85/2.76 (m, 2H; C$_\beta$H), 3.51/3.51 (m, 1H; H$_{c,Allyl}$), 3.28/3.17 (m, 1H; H$_{a/s,Allyl}$), 3.11/2.78 (m, 1H; H$_{a/s,Allyl}$), 1.22/0.80 (m, 1H; H$_{a/s,Allyl}$), 0.99/0.80 (m, 1H; H$_{a/s,Allyl}$); ^{13}C{^{1}H} NMR (100.6 MHz, [D$_6$]DMSO): δ = 230.0/228.8, 228.2/227.9 (CO), 178.2/179.1 (C=O−His), 138.7/140.5 (C−H(His)), 133.5/135.0 (C$_q$−His), 114.7/114.6 (CH−His), 74.2/68.1 (C$_c$−allyl), 60.2/57.8 (C−allyl), 51.7/52.2 (C−allyl), 52.2/52.0 (C$_\alpha$), 28.0/28.0 (C$_\beta$); IR (KBr): $\tilde\nu$ = 3332 (m, NH), 1932 (vs), 1835 (s), 1805 (s, CO), 1615 (m, C=O); IR (MeOH) 1939, 1847 (CO); MS (ESI$^+$, MeOH): 350 [M+H]$^+$, 372 [M+Na]$^+$, 721 [2M+Na]$^+$.

2: Methyl 3-bromopropioniate (1.90 mL, 16.47 mmol) and Cs$_2$CO$_3$ (5.55 g, 17.03 mmol) were added to a solution of **1** (5.90 g, 0.017 mol) in DMF (35 mL). After the mixture had been heated at 80 °C for 2 h, it was filtered,

and then evaporated to dryness. The residue was re-suspended in THF (70 mL), this was then filtered to remove the Cs salts and the THF was removed in vacuo. Purification by preparative HPLC yielded **2** (4.81 g; 65%). Characterization data for **2** are available as supplementary material for reference [20].

3: A suspension of [Mo(2-Me-allyl)(Cl)(CO)$_2$(MeCN)$_2$] (1.64 g, 5.1 mmol) in EtOH (20 mL) was heated in a water bath (50 °C) for 5 – 10 mins, during which time a clear orange-reddish solution formed. A solution of L-histidine (0.79 g, 5.1 mmol) and CsOH·H$_2$O (0.85 g, 5.1 mmol) in H$_2$O (5 mL) was added, resulting in the formation of a small amount of precipitate, which dissolved again upon stirring. After the mixture was stirred at room temperature for 30 min, the solvent was removed in vacuo. The sticky residue was redissolved in EtOH (15 mL) and stirred for 15 mins, resulting in the formation of a yellow precipitate. The solid was isolated by filtration, washed with H$_2$O (5 mL) and diethyl ether (15 mL), and dried in vacuo. Yield: 1.50 g (82%). X-ray quality crystals were obtained by evaporation of a H$_2$O/MeOH (1:3 v/v) solution under a stream of argon. ^{1}H NMR (400.1 MHz, [D$_6$]DMSO): δ = 12.62 (br, 1H; NH), 8.41/7.99 (br, 1H; N$_2$CH$_{Im}$), 6.91 (br, 1H; CH$_{Im}$), 5.04/4.19 (br, 1H; NH$_2$), 3.32 (b, 1H; NH$_2$), 3.28 (br, 2H; C$_\alpha$ + H$_{Allyl}$), 2.91 (m, 2H; C$_\beta$H$_2$), 2.66 (br, 1H; H$_{Allyl}$), 2.66 (br, 1H; H$_{Allyl}$), 1.75 (br, 3H; CH$_3$), 0.80 (br, 2H; H$_{Allyl}$); ^{13}C{^{1}H} NMR (62.9 MHz, [D$_6$]DMSO): δ = 228.2 (b; CO), 178.7 (C = O), 138.9 (b; C$_{Im}$), 134.2 (C$_{Im,q}$), 114.7 (C$_{Im}$), 79.9 (b; C$_{allyl}$), 55.9 (b; C$_{allyl}$), 52.2 (C$_\alpha$), 28.0 (C$_\beta$), 19.3 (CH$_3$); IR (KBr): $\tilde\nu$ = 3323 (m), 3248 (m, NH), 1928 (vs), 1842 (s), 1805 (vs, CO), 1645 (s), 1616 (m, C=O), 1616 (m); IR (MeOH) 1939, 1848 (CO); MS: (FAB$^-$): m/z: 382 [M−H]$^-$.

4: Methyl 3-bromopropioniate (0.8 mL, 7.32 mmol) and Cs$_2$CO$_3$ (1.12 g, 3.4 mmol) were added to a solution of **3** (1.24 g, 3.4 mmol) in DMF (20 mL) and the mixture was heated at 80 °C for 2 h. After the mixture had been allowed to cool down to room temperature, it was filtered. The filtrate was concentrated to dryness in vacuo and re-suspended in THF (35 mL). The suspension was filtered to remove all of the Cs salts, followed by removal of the solvent in vacuo. Purification by preparative HPLC afforded **4** (1.27 g; 83%). Crystals suitable for X-ray analysis were grown by slow evaporation of a MeOH/H$_2$O (1/1 v/v) mixture under a stream of argon. ^{1}H NMR (250.13 MHz, [D$_6$]DMSO): δ = 8.07 (br, 1H; N$_2$CH$_{Im}$), 6.99 (br; CH$_{Im}$), 5.04/4.26 (br, 1H; NH$_2$), 4.26 (br, 2H; N$_\epsilon$CH$_2$), 3.60 (s, 3H; C(O)CH$_3$), 3.34 (br, 1H; NH$_2$), 3.37 (b, 2H; C$_\alpha$H+H$_{Allyl}$), 2.80 (br, 2H; C$_\beta$H$_2$), 2.87 (br, 2H; N$_\epsilon$−CH$_2$CH$_2$), 2.48 (br, 1H; H$_{Allyl}$), 1.71 (br, 3H; Allyl−CH$_3$), 0.80 (b, 2H; H$_{Allyl}$); ^{13}C{^{1}H} NMR (62.9 MHz, [D$_6$]DMSO): δ = 228.5 (b; CO), 178.7 (b; C=O, His), 171.0 (C=O, ester), 140.0 (b; C$_{Im}$), 134.9 (C$_{Im,q}$), 117.5 (C$_{Im}$), 79.2 (b; C$_{allyl}$), 55.8 (b; C$_{allyl}$), 52.0 (C$_\alpha$), 51.6 (C(O)−CH$_3$), 42.5 (N$_\delta$−CH$_2$), 34.5 (N$_\delta$−CH$_2$−CH$_2$), 27.9 (C$_\beta$), 19.2 (CH$_3$); IR (KBr): $\tilde\nu$ = 3311 (m), 3248 (m, NH), 1924 (vs), 1838 (vs), 1816 (vs, CO), 1724 (s, C=O-ester), 1633 (s), 1620 (s, C=O-carboxylate+δ(NH$_2$)); IR(CH$_2$Cl$_2$): $\tilde\nu$ = 1932, 1835 (CO); MS (FAB$^+$) 450 [M+H]$^+$, 899 [2M+H]$^+$, 422 [M−CO+H]$^+$, 394 [M−2CO+H]$^+$; (FAB)$^-$ 448 [M−H]$^-$, 897 [2M−H]$^-$; elemental analysis calcd (%) for C$_{16}$H$_{20}$MoN$_3$O$_6$: C 43.06, H 4.52, N 9.42; found: C 42.95, H 4.61, N 9.28.

[Mo(His)(CO)$_3$]AsPh$_4$ (5): This compound was prepared as reported previously.[22] Crystals of **5**·H$_2$O suitable for X-ray diffraction were grown by slow evaporation of a MeOH/H$_2$O (9:1 v/v) mixture under a stream of argon. IR data are consistent with the literature.[22] ^{1}H NMR (400.13 MHz, [D$_6$]DMSO): δ = 12.13 (b, 1H; NH$_{Im}$) 7.89 (m, 4H; ArH), 7.78 (m, 24H; ArH), 7.62 (s, 1H; N$_2$CH$_{His}$), 6.80 (s, 1H; CH$_{His}$), 3.92 (m, 1H; C$_\alpha$H), 3.39 (m, 1H; NH$_2$), 3.12 (d, ^{2}J(H,H) = 11.0 Hz, 1H; NH$_2$), 2.91 (pseudo-dd, 1H; C$_\beta$H$_2$), 2.79 (pseudo-dd, 1H; C$_\beta$H$_2$); ^{13}C{^{1}H} NMR (100.6 MHz, [D$_6$]DMSO): δ = 233.2 (CO), 229.7 (CO), 178.5 (C=O), 136.5 (N$_2$CH$_{His}$), 135.8 (C$_\gamma$His), 134.3 (C$_{Ar}$), 133.2 (C$_{Ar}$), 130.9 (C$_{Ar}$), 121.0 (C$_{Ar,q}$), 113.5 (CH$_{His}$), 52.4 (C$_\alpha$), 28.8 (C$_\beta$).

X-ray crystallography: Transparent yellow single crystals of **1** and **3** were coated with perfluoropolyether, picked up with glass fibers and mounted on a Nonius Kappa-CCD diffractometer equipped with a rotating Mo anode setup. Yellow crystals of **4** and **5** were mounted on a Siemens SMART diffractometer with a sealed Mo X-ray tube. Both diffractometers were equipped with graphite monochromators (λ(Mo$_{K\alpha}$) = 0.71073) and a cryogenic nitrogen stream operating at 100(2) K. Crystallographic data of the compounds are listed in Table 6. Cell constants were obtained from a least-square fit of the diffraction angles of several thousand strong reflections. Intensity data were corrected for Lorentz and polarization effects. Crystal faces of **5** were determined and the face-indexed correction

routine embedded in ShelXTL[59] was used to account for absorption giving minimum and maximum transmission factors of 0.631 and 0.843, respectively. Intensity data of **4** were corrected by using the semiempirical correction program SADABS,[60] which gave transmission factors of 0.756 and 0.9625. Intensity data of **1** and **3** were left uncorrected. The Siemens ShelXTL software package was used for solution, refinement, and artwork of the structures and neutral atom scattering factors of the program were used. Non-hydrogen atoms were refined anisotropically, and hydrogen atoms, except allyl hydrogen atoms, were placed at calculated positions and refined as riding atoms with isotropic displacement parameters. Allyl hydrogen atoms were located from the difference map and isotropically refined with C−H distances restrained to be equal within errors. CCDC-168288 (**1**), CCDC-168289 (**3**), CCDC-168290 (**4**), and CCDC-168291 (**5**) contain the supplementary crystallographic data for this paper. These data can be obtained free of charge via www.ccdc.cam.ac.uk/conts/retrieving.html (or from the Cambridge Crystallographic Data Centre, 12 Union Road, Cambridge CB2 1EZ, UK; fax: +44 1223/336-033; or deposit@ccdc.cam.ac.uk).

Computational details: Geometries have been fully optimized without symmetry constraints at the BP86/SDD level, that is by employing the exchange and correlation functionals of Becke[61] and Perdew,[62, 63] respectively, together with a fine integration grid (75 radial shells with 302 angular points per shell), and the Stuttgart–Dresden relativistic effective core potentials with the corresponding valence basis sets for Mo (6s5p3d),[64] C, N, and O (valence double-zeta),[65] and Dunning's double-zeta basis for H.[66] The nature of the stationary points has been verified by computations of the harmonic frequencies at that level. Each transition state has been characterized by the occurrence of a single imaginary frequency and by visual inspection of the corresponding vibrational mode, in order to ensure that the desired minima are connected. Subsequently, single-point energy calculations for these BP86/SDD geometries have been performed at the BPW91/II″ level, that is by using the functionals of Becke,[61] Perdew, and Wang,[67, 68] a (16s10p9d) all-electron basis for Mo, contracted from the well-tempered 22s14p12d set of Huzinaga and Klobukowski[69] and augmented with two d shells of the well-tempered series, and standard 6-31 G* basis set[70, 71] for all other elements. This level is denoted BPW91/II″//BP86/SDD. Unless otherwise noted, energies are

reported at this level, including the BP86/SDD zero-point corrections. The same methods, together with more extended basis sets on the ligands, have proven to be well suited for a description of reactivities and ⁹⁵Mo chemical shifts of a number of inorganic and organometallic molybdenum compounds,[72] and are among those DFT-based methods that are now routinely used to study many aspects of transition-metal chemistry.[73] Open-shell systems were treated with the unrestricted Kohn–Sham formalism, and no significant spin contamination was found. All computations employed the Gaussian 98 program package[74] and have been carried out on Compaq XP1000 workstations at the Max-Planck-Institut für Kohlenforschung, Mülheim.

Acknowledgements

[1] S. J. Lippard, J. M. Berg, *Principles of Bioinorganic Chemistry*, University Science Books, Mill Valley, California, **1994**.

[2] W. Kaim, B. Schwederski, *Bioanorganische Chemie*, B. G. Teubner, Stuttgart, **1995**.

[3] A. Almenningen, A. Haaland, S. Samdal, *J. Organomet. Chem.* **1978**, *149*, 219–229.

[4] N. Hebendanz, F. H. Köhler, G. Müller, J. Riede, *J. Am. Chem. Soc.* **1986**, *108*, 3281–3289.

Table 6. Summary of the crystallographic data for **1**·MeOH, **3**, **4**, and **5**·H₂O.

	1·MeOH	**3**	**4**	**5**·H₂O
empirical formula	$C_{12}H_{17}MoN_3O_5$	$C_{12}H_{15}MoN_3O_4$	$C_{16}H_{21}MoN_3O_6$	$C_{33}H_{30}AsMoN_3O_6$
formula weight	379.23	361.21	447.30	735.46
T [K]	100(2)	100(2)	100(2)	100(2)
λ [Å]	0.71073	0.71073	0.71073	0.71073
crystal size [mm]	$0.35 \times 0.32 \times 0.32$	$0.32 \times 0.14 \times 0.04$	$0.52 \times 0.35 \times 0.28$	$0.40 \times 0.28 \times 0.12$
crystal system	trigonal	monoclinic	orthorhombic	monoclinic
space group	$P3_121$ (no. 152)	$P2_1$ (no. 4)	$P2_12_12_1$ (no. 19)	$P2_1$ (no. 4)
a [Å]	11.7007(6)	8.5602(12)	8.5384(4)	7.7734(6)
b [Å]	11.7007(6)	12.704(2)	11.7713(8)	13.8012(10)
c [Å]	18.9244(11)	12.667(2)	17.9943(12)	14.7311(11)
α [°]	90	90	90	90
β [°]	90	92.05(2)	90	94.43(2)
γ [°]	120	90	90	90
V [Å³]	2243.8(2)	1376.6(4)	1808.6(2)	1575.7(2)
Z	6	4	4	2
ρ_{calcd} [g cm⁻³]	1.684	1.743	1.643	1.550
μ(Mo$_{K\alpha}$) [mm⁻¹]	0.901	0.969	0.763	1.507
θ range [°]	$2.01 \leq \theta \leq 27.40$	$3.21 \leq \theta \leq 27.49$	$2.07 \leq \theta \leq 33.15$	$2.02 \leq \theta \leq 27.50$
index ranges	$\pm h, \pm k, \pm l$	$\pm h, \pm k, \pm l$	$\pm h, \pm k, \pm l$	$\pm h, \pm k, \pm l$
data collected	24508	17552	19891	13513
independent data	3402 [$R_{int} = 0.0639$]	6219 [$R_{int} = 0.1373$]	6703 [$R_{int} = 0.0235$]	5701 [$R_{int} = 0.0449$]
observed data[$I > 2\sigma(I)$]	3268	5419	6314	4960
data/restraints/parameters	3402/6/238	6219/9/387	6700/6/249	5701/2/403
goodness-of-fit on F^2[a]	1.049	1.017	1.036	1.047
final R_1 (obs. data)[b]	0.0223	0.0554	0.0222	0.0346
final wR_2 (all data)[c]	0.0527	0.1349	0.0519	0.0835
largest diff. peak/hole [e Å⁻³]	0.496/ − 0.409	1.046/ − 0.926	0.451/ − 0.442	1.007/ − 0.704

[a] GooF = $[\Sigma[w(F_o^2 - F_c^2)^2]/(n - p)]^{1/2}$ where n = no. of reflections and p = no. of refined parameters. [b] $R1 = \Sigma||F_0| - |F_c||/\Sigma|F_0|$. [c] w$R2 = [\Sigma[w(F_o^2 - F_c^2)^2]/\Sigma[w(F_o^2)_2]]^{1/2}$, where $w = 1/\sigma^2(F_o^2) + (aP)^2 + bP$, $P = (F_o^2 + 2F_c^2)/3$.

[5] H. Sitzmann, *Coord. Chem. Rev.* **2001**, *215*, 287 – 327.

[6] K. H. Theopold, *Acc. Chem. Res.* **1990**, *23*, 263 – 270.

[7] P. W. Jolly, *Acc. Chem. Res.* **1996**, *29*, 544 – 551.

[8] K. H. Theopold, *Eur. J. Inorg. Chem.* **1998**, 15 – 24.

[9] D. Astruc, *Angew. Chem.* **1988**, *100*, 662 – 680; *Angew. Chem. Int. Ed. Engl.* **1988**, *27*, 643 – 650.

[10] J. Ruiz, F. Ogliaro, J. Y. Saillard, J. F. Halet, F. Varret, D. Astruc, *J. Am. Chem. Soc.* **1998**, *120*, 11 693 – 11 705.

[11] H. A. Trujillo, C. M. Casado, J. Ruiz, D. Astruc, *J. Am. Chem. Soc.* **1999**, *121*, 5674 – 5686.

[12] N. G. Connelly, W. E. Geiger, S. R. Lovelace, B. Metz, T. J. Paget, R. Winter, *Organometallics* **1999**, *18*, 3201 – 3207.

[13] N. G. Connelly, W. E. Geiger, *Chem. Rev.* **1996**, *96*, 877 – 910.

[14] R. Poli, *Chem. Rev.* **1996**, *96*, 2135 – 2204.

[15] R. Poli, *Acc. Chem. Res.* **1997**, *30*, 494 – 501.

[16] R. Poli, L.-S. Wang, *Coord. Chem. Rev.* **1998**, *180*, 169 – 189.

[17] M. A. Bennett, G. A. Heath, D. C. R. Hockless, I. Kovacik, A. C. Willis, *J. Am. Chem. Soc.* **1998**, *120*, 932 – 941.

[18] F. Ogliaro, J. F. Halet, D. Astruc, J. Y. Saillard, *New J. Chem.* **2000**, *24*, 257 – 259.

[19] L.-S. Wang, J. C. Fettinger, R. Poli, *J. Am. Chem. Soc.* **1997**, *119*, 4453 – 4464.

[20] D. R. van Staveren, E. Bothe, T. Weyhermüller, N. Metzler-Nolte, *Chem. Commun.* **2001**, 131 – 132.

[21] W. Beck, W. Petri, H.-J. Meder, *J. Organomet. Chem.* **1980**, *191*, 73 – 77.

[22] H.-J. Meder, W. Beck, *Z. Naturforsch. B* **1986**, *41*, 1247 – 1254.

[23] A. Hess, O. Brosch, T. Weyhermüller, N. Metzler-Nolte, *J. Organomet. Chem.* **1999**, *589*, 75 – 84.

[24] A. Hess, J. Sehnert, T. Weyhermüller, N. Metzler-Nolte, *Inorg. Chem.* **2000**, *39*, 5437 – 5443.

[25] O. Brosch, T. Weyhermüller, N. Metzler-Nolte, *Inorg. Chem.* **1999**, *38*, 5308 – 5313.

[26] O. Brosch, T. Weyhermüller, N. Metzler-Nolte, *Eur. J. Inorg. Chem.* **2000**, 323 – 330.

[27] A. Hess, N. Metzler-Nolte, *Chem. Commun.* **1999**, 885 – 886.

[28] J. C. Verheijen, G. A. van der Marel, J. H. van Boom, N. Metzler-Nolte, *Bioconjugate Chem.* **2000**, *11*, 741 – 743.

[29] D. R. van Staveren, T. Weyhermüller, N. Metzler-Nolte, *Organometallics* **2000**, *19*, 3730 – 3735.

[30] J. W. Faller, M. J. Incorvia, *Inorg. Chem.* **1968**, *7*, 840 – 842.

[31] A. Davison, W. C. Rode, *Inorg. Chem.* **1967**, *6*, 2124 – 2125.

[32] M. L. H. Green, *J. Organomet. Chem.* **1995**, *500*, 127 – 148.

[33] J. W. Faller, B. C. Whitmore, *Organometallics* **1986**, *5*, 752 – 755.

[34] K.-B. Shiu, K.-S. Liou, C. P. Cheng, B.-R. Fang, Y. Wang, G.-H. Lee, W.-J. Vong, *Organometallics* **1989**, *8*, 1219 – 1224.

[35] P. Espinet, R. Hernando, G. Iturbe, F. Villafañe, A. G. Orpen, I. Pascual, *Eur. J. Inorg. Chem.* **2000**, 1031 – 1038.

[36] B. J. Brisdon, K. A. Conner, R. A. Walton, *Organometallics* **1983**, *2*, 1159 – 1163.

[37] B. Brisdon, S. K. Enger, M. J. Weaver, R. A. Walton, *Inorg. Chem.* **1987**, *26*, 3340 – 3344.

[38] M. D. Curtis, O. Eisenstein, *Organometallics* **1984**, *3*, 887 – 895.

[39] B. J. Brisdon, A. A. Woolf, *J. Chem. Soc. Dalton Trans.* **1978**, 291 – 295.

[40] J. W. Faller, D. A. Haitko, R. D. Adams, D. F. Chodosh, *J. Am. Chem. Soc.* **1979**, *101*, 865 – 876.

[41] K.-B. Shiu, C.-J. Chang, S.-L. Wang, F.-L. Liao, *J. Organomet. Chem.* **1991**, *407*, 225 – 235.

[42] B. J. Brisdon, M. Cartwright, A. G. W. Hodson, M. F. Mahon, K. C. Molloy, *J. Organomet. Chem.* **1992**, *435*, 319 – 335.

[43] C. Borgmann, C. Limberg, L. Zsolnai, *Chem. Commun.* **1998**, 2729 – 2730.

[44] D. A. Cooper, S. J. Rettig, A. Storr, J. Trotter, *Canad. J. Chem.* **1986**, *64*, 1643 – 1651.

[45] A. J. Graham, R. H. Fenn, *J. Organomet. Chem.* **1970**, *25*, 173 – 191.

[46] E. M. Holt, S. L. Holt, K. J. Watson, *J. Chem. Soc. Dalton Trans.* **1973**, 2444 – 2447.

[47] S. J. Rettig, A. Storr, J. Trotter, *Canad. J. Chem.* **1988**, *66*, 97 – 100.

[48] M. D. Curtis, N. A. Fotinos, *J. Organomet. Chem.* **1984**, *272*, 43 – 54.

[49] Note that Mo(1)−C(40) and Mo(1)−C(50) are just within 3σ, whereas this is not the case with Mo(1)−C(30) and Mo(1)−C(50).

[50] At the BPW 91/II//BP86/ECP 1 level (which uses larger basis sets on the ligands), virtually the same energy difference is obtained, 1.7 kJ mol⁻¹. Thus, the results do not appear to be very sensitive to the basis set employed.

[51] A similar path with two consecutive pseudorotations according to the sequence **a-c-b** was computed to be less favorable for **1** (highest point **TS 3 cb**, 69 kJ mol⁻¹, not shown in Scheme 4) and even more so for **3** (**TS 3 cb**, 95 kJ mol⁻¹).

[52] M. Brookhart, M. L. H. Green, *J. Organomet. Chem.* **1983**, *250*, 395 – 408.

[53] P. S. Braterman, *Metal Carbonyl Spectra*, Academic Press, London, **1975**.

[54] P. S. Braterman, *Struct. Bond.* **1972**, *10*, 57 – 86.

[55] P. S. Braterman, *Struct. Bond.* **1976**, *26*, 1 – 42.

[56] T. E. Bitterwolf, J. T. Bays, B. Scallorn, C. A. Weiss, M. W. George, I. G. Virrels, J. C. Linehan, C. R. Yonker, *Eur. J. Inorg. Chem.* **2001**, 2619 – 2624.

[57] C. Limberg, A. J. Downs, T. M. Greene, T. Wistuba, *Eur. J. Inorg. Chem.* **2001**, 2613 – 2618.

[58] H. tom Dieck, H. Friedel, *J. Organomet. Chem.* **1968**, *14*, 375 – 385.

[59] ShelXTL, Siemens Analytical X-ray Instruments, **1994**.

[60] SADABS, G. M. Sheldrick, University of Göttingen, Göttingen, **1994**.

[61] A. D. Becke, *Phys. Rev. A* **1988**, *38*, 3098 – 3100.

[62] J. P. Perdew, *Phys. Rev. B* **1986**, *33*, 8822 – 8824.

[63] J. P. Perdew, *Phys. Rev. B* **1986**, *34*, 7406.

[64] D. Andrae, U. Häußermann, M. Dolg, H. Stoll, H. Preuß, *Theor. Chim. Acta* **1990**, *77*, 123 – 141.

[65] A. Bergner, M. Dolg, W. Küchle, H. Stoll, H. Preuß, *Mol. Phys.* **1993**, *80*, 1431 – 1441.

[66] T. H. Dunning, *J. Chem. Phys.* **1970**, *53*, 2823 – 2833.

[67] J. P. Perdew, *Electronic Structure of Solids*, Akademie Verlag, Berlin, **1991**.

[68] J. P. Perdew, Y. Wang, *Phys. Rev. B* **1992**, *45*, 13 244 – 13 249.

[69] S. Huzinaga, M. Klobukowski, *J. Mol. Struct. (THEOCHEM)* **1988**, *167*, 1 – 210.

[70] P. C. Hariharan, J. A. Pople, *Theor. Chim. Acta* **1973**, *28*, 213 – 222.

[71] W. J. Hehre, R. Ditchfield, J. A. Pople, *J. Chem. Phys.* **1972**, *56*, 2257 – 2261.

[72] M. Bühl, *Chem. Eur. J.* **1999**, *5*, 3514 – 3522.

[73] W. Koch, M. C. Holthausen, *A Chemist's Guide to Density Functional Theory*, Wiley-VCH, Weinheim, **2000**.

[74] Gaussian 98, M. J. Frisch, G. W. Trucks, H. B. Schlegel, G. E. Scuseria, M. A. Robb, J. R. Cheeseman, V. G. Zakrzewski, J. A. Montgomery, R. E. Stratman, J. C. Burant, S. Dapprich, J. M. Millam, A. D. Daniels, K. N. Kudin, M. C. Strain, O. Farkas, J. Tomasi, V. Barone, M. Cossi, R. Cammi, B. Mennucci, C. Pomelli, C. Adamo, S. Clifford, J. Ochterski, G. A. Petersson, P. Y. Ayala, Q. Cui, K. Morokuma, D. K. Malick, A. D. Rabuck, K. Raghavachari, J. B. Foresman, J. Cioslowski, J. V. Ortiz, A. G. Baboul, B. B. Stefanov, C. Liu, A. Liashenko, P. Piskorz, I. Komaromi, R. Gomperts, R. L. Martin, D. J. Fox, T. Keith, M. A. Al-Laham, C. Y. Peng, A. Nanayakkara, C. Gonzalez, M. Challacombe, P. M. W. Gill, B. G. Johnson, W. Chen, M. W. Wong, J. L. Andres, C. Gonzales, M. Head-Gordon, E. S. Replogle, J. A. Pople, Gaussian Inc., Pittsburgh PA, **1998**.